Multiple-time-scale analysis of nonlinear modes in ferroelectric $LiNbO_3$

A. K. Bandyopadhyay,[1,*] P. C. Ray,[2,†] Loc Vu-Quoc,[3,‡] and Arthur R. McGurn[4,§]
[1]*Govt. College of Engineering & Ceramic Technology, W. B. University of Technology, 73, A. C. Banerjee Lane, Calcutta 700010, India*
[2]*Department of Mathematics, Govt. College of Engineering & Leather Technology, LB Block, Sector III, Salt Lake, Calcutta 700098, India*
[3]*Department of Mechanical & Aerospace Engineering, University of Florida, Gainesville, Florida 32611, USA*
[4]*Department of Physics, Western Michigan University, Kalamazoo, Michigan 49008-5252, USA*
(Received 2 August 2007; revised manuscript received 23 December 2009; published 3 February 2010; publisher error corrected 12 February 2010)

A model of a ferroelectric crystal in terms of a one-dimensional array of ferroelectric slab domains is treated theoretically for the dynamics of the "array of domains." Two approaches are considered. In a first, the system is treated within a continuum limit in which the space and time evolution of the polarization of the crystal are described by a nonlinear Klein-Gordon equation. A multiple-time-scale analysis is used to determine the linear and nonlinear parts of the frequencies of the extended modes of oscillation of the array. An application is also made to study these modes in the presence of impurities in inhomogeneous ferroelectric materials such as lithium niobate. In a second approach, the discrete equations for the coupling of neighboring ferroelectric slab domains are used to study intrinsic localized modes of the ferroelectric crystal. These are highly localized modes that arise from their self-consistent interactions with the nonlinearity of the system.

DOI: 10.1103/PhysRevB.81.064104 PACS number(s): 77.80.Dj, 77.84.Ek, 77.90.+k

I. INTRODUCTION

Ferroelectricity is an important property of solids, arising in crystal systems undergoing structural changes below a critical temperature, leading to the development of a spontaneous polarization.[1–8] The transition is either first or second order and is roughly described by an appropriate Landau-Ginzburg free energy. Real ferroelectrics occur as collections of domains of pure ferroelectric behavior where the ferroelectric domains (as with ferromagnetic domains) are created and oriented by a need to minimize the free energy of the crystal and fields. The bulk properties and domain structure of these materials are among the classic systems treated in statistical physics and have been extensively studied. Recently, however, they have gained renewed interest for potential applications in nanoscience and the design of nanodevices, where the focus is on properties exhibited at small length scales.[3–12] The new applications are based both on classic ferroelectric properties and features particular to nanostructured arrays and include applications to:[9] (1) generating high dielectric coefficients over wide ranges of temperatures and frequencies in the design of integrated or surface mounted device capacitors, (2) using large piezoelectric effects in electromechanical sensors, actuators, and transducers, (3) utilization of materials with high pyroelectric coefficients for infrared sensors, (4) using semiconductor ferroelectrics in tunable thermistors and in positive temperature coefficient resistors, (5) utilization of nonlinear dielectric materials with field tunable permittivities and refractive indices in electromechanical devices. These current interests warrant a more detailed look at the dynamical properties of domain arrays which may become significant features at some of the length scales of interest and this aspect is definitely very important.

In this paper the dynamical properties of the domain structure of a ferroelectric crystal such as lithium niobate are studied. The focus is on a simple model of an idealized one-dimensional layered array of domains which has been treated in a number of previous publications.[1,5,7,8] In these treatments a discrete model for the interacting domains was developed and then reformulated into a continuum model. The two formulations become of interest depending on the characteristic length scale of domain excitations compared to typical lengths of the domains and on the number of domains forming the array. Originally these efforts focused on a study of the properties of the static system.[1,5,7] Later, the continuum model was applied to a stability analysis of solitons of different velocities in the domain arrays.[8]

Both the discrete and continuum models are based on generalizing the Landau-Ginzburg free-energy form for ferroelectric materials. The discrete model treats domain arrays in which each domain has a uniform polarization over the finite region of the domain volume[1,5,7,8] and the polarizations of neighboring domains are oppositely directed. This is convenient when the length scales of the excitations in the system are comparable to the domain sizes. The continuum model treats the staggered polarization as slowly varying over a neighborhood of several domains so that the domains are treated as a staggered polarization density. The continuum model reformulation is accomplished applying to the discrete model a Taylor expansion in the domain slab thickness which is valid for long-wavelength excitations in arrays consisting of a large number of domains.[7,8] The dynamical equation of the continuum model has the form of a nonlinear Klein-Gordon (K-G) equation for the staggered polarization of the system as a function of time and the space variables perpendicular to the ferroelectric domain slabs.

In a first study, for the extended (i.e., plane-wavelike) modes of the array, the continuum model is treated to determine the renormalization of the mode frequencies with mode amplitude due to the system nonlinearity. The time dependence of the domain array is obtained using multiple-time-scale analysis (MTSA) methods.[13] The plane-wavelike

 ©2010 The American Physical Society

modes of the nonlinear system are found to evolve from those of the linear limit of the system such that the nonlinear component of the interactions adds a complicated renormalization of their properties. The effects of impurities in the system on this renormalization are considered using recent data on lithium niobate.[11,12] These effects are of interest as they occur in many ferroelectrics and may have applications in nonlinear optical communications.

Within the continuum limit dynamics, the nonlinear Klein-Gordon equation with second-order space and time derivatives has been used in a number of studies on domain walls, the motion of domain walls, and in some preliminary treatments of arrays of domains (see Ref. 8 and references therein). It has also been mentioned in our previous analysis of these systems for the limiting case in which the spatial term in the Klein-Gordon equation vanishes and the resulting system equation reduces to the nonlinear Duffing oscillator equation.[7,10] A particular facility in these treatments is that the K-G equation is a well-known equation of mathematical physics which exhibits a wide variety of interesting properties and has had applications to a wide variety of different physical systems. Our treatment here of the dynamical properties of the extended modes of the Klein-Gordon equation involves a MTSA. The MTSA and its applications in the study of various mechanical systems have been extensively discussed by Nayfeh,[13] and more recently Das *et al.*[14] have presented an interesting treatment of these techniques for linear and nonlinear mechanical vibration analysis. The MTSA allows for a determination of the frequency and amplitude of the modes as an expansion in a series of relevant increasing time scales, revealing both the linear limit and the nonlinear corrections of the frequencies. It overcomes problems with singularities that arise in the traditional perturbation expansion in the nonlinearity of the system as a small parameter.

In a second study, a set of intrinsic localized modes (ILMs) of the domain array will be investigated. These are highly localized pulses in space and are found in the discrete nonlinear model formulation. Unlike the plane-wavelike modes, ILMs have no counterparts in the linear system, but exist only because of the system nonlinearity in a periodic lattice.[15–17] They are formed as a self-consistent interaction between the mode and the system nonlinearity so that an ILM modifies the local properties of the system at the ILM peak through the system nonlinearity, and the modified local properties of the system provide the environment for the ILM to exist. The existence of ILM have been proposed theoretically in a wide variety of discrete many-body systems, and they have been observed experimentally in a number of different types of such systems.[16] Detailed discussions of ILM have been reviewed extensively in the works of Sievers *et al.*[16,17] and Segev and co-workers.[15] For our discussions we use a simple and general formulation given originally by Sievers and Page[17] for the treatment of ILM in nonlinear vibrational systems. The formulation is appropriate to highly localized pulses having widths that are not large compared to the domain widths so that the continuum limit formulation cannot be applied to their study.

Some important works (in a nonexhaustive literature search) related to the above proposed direction of research are now briefly mentioned. These focus mainly on bulk properties of pure and impure ferroelectric systems and with the nature of intrinsic localized modes compared to the continuum limit soliton solutions. From a theoretical standpoint, Corso and co-workers[18] did an extensive study using density-functional perturbation theory of the dynamics of lattices in a variety of materials, including ferroelectrics. They employed a nonlinear approach, mainly evaluating the exchange and correlation energy, to determine the nonlinear optical susceptibility of a material at low frequency.[19] The phonon-dispersion relation of ferroelectrics was also studied extensively by Ghosez *et al.*[20,21] These studies, however, were related more to understanding the structure and metal-oxygen bonds of certain ferroelectric materials rather than to a determination of the domain modes of vibration or soliton motion in the system. Comparisons of nonlinear treatments of localized modes in continuum and discrete systems, however, were made by Kivshar *et al.*[22,23] giving an impressive study of "intrinsic localized modes," i.e., so-called lattice solitons and their oscillations in a discrete system. These studies were based on the perturbed nonlinear Schrodinger equation and the Peirls-Nabarro potential. They showed that some of the properties of the discrete nonlinear lattices, e.g., modulation instability of continuous wave solutions, are exhibited through some of the novel features that are introduced solely by the "discreteness"[23] (see the references therein). An impressive work by Willis' group on the nonlinear response of the sine-Gordon equation to an ac field[24] is also noted in this context. From an experimental standpoint, anharmonic vibrations were experimentally dealt with by Brennan and Nelson[25] in both lithium niobate and lithium tantalate crystals through "impulsive" stimulated Raman scattering measurements (see the references therein). In addition, for localized modes an extensive description of ILM and the implication of discreteness for such modes have been recently given by a voluminous review by Flach and Gorbach.[26]

In Sec. II, a review of the discrete model system and its Hamiltonian is given. The time-dependent continuum limit (nonlinear Klein-Gordon equation) is obtained and discussed. In Sec. III, the nonlinear dispersion relation of the plane-wavelike modes of the array of domains is obtained using the MTSA. This is followed by a treatment of ILM in the discrete system. In Sec. IV, results are presented for parameters appropriate to lithium niobate. Conclusions are given in Sec. V.

II. MODEL

We consider an idealized model of a one-dimensional array of N identical ferroelectric domains layered along the x axis[1,5,7,8] (see Fig. 1). In the ground state the array of polarized domains is antiferroelectrically ordered. The domains are rectangular parallelepipeds of length L_1 in the x direction, of height $d \ll NL_1$ in the z direction, and translationally invariant in the y direction. Between neighboring domains are domain walls of length $W_L \ll L_1$, d, and the total length of the array along the x direction is $L_2 = NL_1$. For simplicity the polarization of each domain is oriented along the z axis and denoted in the ith domain by $\tilde{P}_i$. The polarization vector $\tilde{P}_i$

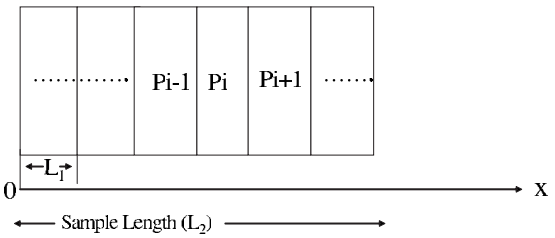

FIG. 1. Schematic of the polarization domains in the discrete case. The lengths of the domains along the x axis are L_1, the length of the array is $L_2=NL_1$, and the domain walls are lines.

can be either positive or negative to indicate an orientation along the + or $-z$ axis and can be expressed in terms of a slowly varying staggered polarization, P_i, as $\tilde{P}_i=(-1)^i P_i$.

In a previous treatment a time-dependent formulation for the dynamics of the domain array was obtained as a generalization of the Landau-Ginzburg free-energy form[1,7]

$$G = -\alpha_1 P^2/2 + \alpha_2 P^4/4 - E_0 P \tag{1}$$

for a uniform single-domain ferroelectric. The nearest-neighboring domains were taken to interact by a harmonic potential with a phenomenological spring constant k so that the resulting Hamiltonian for the staggered polarization is given by:[7]

$$H = \frac{1}{2m_d}\sum_{i=1}^{N} p_i^2 + \sum_{i=1}^{N}\left[-\frac{\alpha_1 Q_d^2}{2}\left(\frac{P_i}{Q_d}\right)^2 + \frac{\alpha_2 Q_d^4}{4}\left(\frac{P_i}{Q_d}\right)^4\right] + \sum_{i=1}^{N}\left[\frac{kQ_d^2}{4}\left(\frac{P_i}{Q_d}-\frac{P_{i-1}}{Q_d}\right)^2 - Q_d\left(\frac{P_i}{Q_d}\right)[E_0' + (-1)^{i+1}E_1']\right]. \tag{2}$$

Here

$$p_i = \left(\frac{m_d}{Q_d}\right)\dot{P}_i, \tag{3}$$

where Q_d and m_d are phenomenological inertial constants set by the response of the ferroelectric domains to a perturbation of the P_i, E_0' is a staggered electric field, and E_1' is an applied external electric field.

Equation (2) gives a good general treatment of the mode dynamics in the array, particularly for modes which are strongly localized over a small number of the domains in the array. For extended modes and modes which are localized, and slowly range over a large number of consecutive domains, Eq. (2) can be approximated by a continuum treatment. In this limit, expressed in dimensionless units, Eq. (2) yields a nonlinear Klein-Gordon equation with an ac driving and staggered field given by:[7,8]

$$\frac{\partial^2 P}{\partial t^2} - \bar{k}\frac{\partial^2 P}{\partial x^2} + \bar{\gamma}\frac{\partial P}{\partial t} - \bar{\alpha}_1 P + \bar{\alpha}_2 P^3 - [E_0 + E_1 \sin(n\pi)]\cos(\Omega t) = 0 \tag{4}$$

for the dynamics of the staggered polarization $P(x,t)$. Here $0 \le x \le N$ is the position in the array measured in units of L_1; $P(x,t)=P'(x,t)/P_s$, where $P'(x,t)$ is the polarization at x of the ith domain, where $i-1 \le x/L_1 \le i$ and P_s is the saturation polarization of the ferroelectric; $t=t'/t_c$, where t' is the time and $t_c=\frac{1}{Q_d}\sqrt{\frac{m_d P_s}{E_c}}$ is the characteristic time constant for perturbations of the equilibrium polarization to relax; and $\bar{\alpha}_1 = \alpha_1 P_s/E_c$ and $\bar{\alpha}_2=\alpha_2 P_s^3/E_c$, where E_c is the coercive field of the P-E ferroelectric hysteresis curve.[4] The coefficients associated with the variation in the second-order spatial term and that for first-order time variation in Eq. (4) are given by

$$\bar{k} = \frac{kP_s}{2E_c} \tag{5}$$

and

$$\bar{\gamma} = \frac{\gamma P_s}{t_c E_c}, \tag{6}$$

where γ is a decay constant relating the loss of polarization due to internal friction during its motion in the system, and the fields have been normalized such that $E_0=\frac{E_0'}{E_c}$ and $E_1 = \frac{E_1'}{E_c}$. In addition, in our later discussions of lithium niobate we will take $\alpha_1=\alpha_2 P_s^2$ in Eq. (4) which is appropriate for bulk lithium niobate at room temperature.

III. MULTIPLE-TIME-SCALE ANALYSIS

A. Defining terms

The MTSA is a perturbation-theory approach for the dynamics of nonlinear oscillator equations based on observations originally put forth in the Lindstedt-Poincare technique.[13] Specifically, it is found that in an expansion in the small nonlinearity of the system the nonlinearity of the frequency of the oscillator must explicitly be taken into account in the course of the calculation. Otherwise a poorly behaved perturbation series is obtained.

If ε is a small parameter characterizing the nonlinearity in Eq. (4), then the MTSA formally treats the staggered ferroelectric polarization $P(x,\varepsilon,t)$ as a function of multiple time scales $P(x,\varepsilon,t_0,t_1,t_2,\ldots,t_n)$, where the t_i are defined by[13,14]

$$t_0 = t, \quad t_1 = \varepsilon t, \ldots, \quad t_n = \varepsilon^n t, \ldots \tag{7}$$

For the system in Eq. (4) the small parameter is taken to be proportional to the mode amplitude. In addition, the staggered polarization is also expanded in ε of the form

$$P = P_0 + \varepsilon P_1 + \varepsilon^2 P_2 + \varepsilon^3 P_3 + \cdots, \tag{8}$$

where $P_0=\sqrt{\frac{\bar{\alpha}_1}{\bar{\alpha}_2}}$ is the equilibrium staggered polarization and the P_i's for $i>0$ are functions of $x,t_0,t_1,\ldots,t_n$, etc., describing fluctuations about the equilibrium system. A solution for $P(x,\varepsilon,t_0,t_2,\ldots)$ is then obtained using Eqs. (7) and (8) in Eq. (4). This gives an expansion in ε for $P(x,\varepsilon,t)$, correctly handling the nonlinear oscillator frequency, and avoiding an ill-behaved perturbation series.

Applying the MTSA to Eq. (4), the partial derivative with respect to t becomes

$$\frac{\partial}{\partial t} = \frac{\partial}{\partial t_0}\frac{\partial t_0}{\partial t} + \frac{\partial}{\partial t_1}\frac{\partial t_1}{\partial t} + \cdots = D_0 + \varepsilon D_1 + \varepsilon^2 D_2 + \cdots, \tag{9}$$

where the time differential operators are defined as follows: $D_0 = \partial/\partial t_0$, $D_1 = \partial/\partial t_1$, $D_2 = \partial/\partial t_2$, etc. The second partial derivative in t is then given by

$$\frac{\partial^2}{\partial t^2} = D_0^2 + 2\varepsilon D_1 D_0 + \varepsilon^2(D_1^2 + 2D_0 D_2) + \mathrm{O}(\varepsilon^3) \tag{10}$$

Using Eq. (8) through Eq. (10) in Eq. (4), we find

$$\begin{aligned}(D_0^2 + 2\varepsilon D_1 D_0 + \cdots)(P_0 + \varepsilon P_1 + \varepsilon^2 P_2 + \cdots) - \bar{k}\left(\varepsilon\frac{\partial^2 P_1}{\partial x^2}\right. \\ \left. + \varepsilon^2\frac{\partial^2 P_2}{\partial x^2} + \cdots\right) + \hat{\gamma}\varepsilon^2(D_0 + \varepsilon D_1 + \cdots)(P_0 + \varepsilon P_1 + \varepsilon^2 P_2 \\ + \cdots) - \bar{\alpha}_1(P_0 + \varepsilon P_1 + \varepsilon^2 P_2 + \cdots) + \bar{\alpha}_2(P_0 + \varepsilon P_1 + \varepsilon^2 P_2 \\ + \cdots)^3 - [\hat{E}_0 + \hat{E}_1 \sin(\pi x)]\varepsilon^3 \cos(\Omega t_0) = 0.\end{aligned} \tag{11}$$

Here we have taken $\bar{\gamma}$, E_0, and E_1 to be of the following form: $\bar{\gamma} = \hat{\gamma}\varepsilon^2$, $E_0 = \hat{E}_0\varepsilon^3$, and $E_1 = \hat{E}_1\varepsilon^3$. This assumes a weak interaction of the fields with the system, along with a weak decay rate measured by $\bar{\gamma}$, and is consistent with our $\varepsilon \to 0$ discussions involving these parameters in Eq. (6) of our previous work.[7] In addition, the driving external electric field in Eq. (11) is assumed to have an ac driving frequency Ω of the form $\Omega = \omega + \varepsilon^2\Omega_0 + \cdots$. For example, taking terms of second order, the cosine term in Eq. (11) becomes

$$\cos(\omega t_0 + \varepsilon^2\Omega_0 t_0) = \cos(\omega t_0 + \Omega_0 t_2) = \frac{1}{2}[e^{i(\omega_0 + \Omega_0 t_2)} + \text{c.c.}]. \tag{12}$$

We now investigate the perturbation series obtained from Eqs. (11) and (12), solving the system in powers of ε. In our treatment we begin by assuming that the coefficient $P_1(x, t_0, t_1, \ldots)$ in Eqs. (8) and (11) has the general form

$$P_1 = [A(t_1, t_2, \ldots)\exp(i\omega t_0) + A^*(t_1, t_2, \ldots)\exp(-i\omega t_0)]X_1(x). \tag{13}$$

B. Linear analysis, terms of order ε

Collecting the lowest order terms (terms of order ε) in Eq. (11) gives

$$D_0^2 P_1 - \bar{k}\frac{\partial^2 P_1}{\partial x^2} - \bar{\alpha}_1 P_1 + 3\bar{\alpha}_2 P_0^2 P_1 = 0 \tag{14}$$

for $P_1(x, t_0, t_1, \ldots)$ subject to the vanishing of the polarization at the ends of the ferroelectric domain array, i.e., $P(x = 0, t_0, \ldots) = \mathrm{P}(x = N, t_0, \ldots) = 0$. The solutions of Eq. (14) give the linear limit of the modes of the system with frequencies independent of ε. A solution satisfying the boundary conditions is

$$P_1 = [A(t_1)\exp(i\omega t_0) + A^*(t_1)\exp(-i\omega t_0)]\sin\left(\frac{n\pi x}{N}\right), \tag{15}$$

where $n = 1, 2, 3, \ldots$, $X_1(x) = \sin(\frac{n\pi x}{N})$, and

$$\omega = \left[2\bar{\alpha}_1 + \left(\frac{n\pi}{N}\right)^2\bar{k}\right]^{1/2} \tag{16}$$

gives the "dispersion relation" of the nth linear mode.

It is known from previous studies[7,8] that the Landau coefficients, $\bar{\alpha}_1$ and $\bar{\alpha}_2$, are important in determining the dynamics and stability of both the general polarization modes and the soliton modes that are generated within ferroelectric systems.[7,8] It is not surprising that the above treatment of the linear limits of our system through MTSA shows that $\bar{\alpha}_1$ and $\bar{\alpha}_2$ determine the regions of standing-wave and decaying-wave solutions in a fundamental way. We now turn to the treatment of the nonlinear modes which have higher order terms in ε and to a determination of how the coefficients of the Landau equation affect the physics generated in these terms.

C. Nonlinear analysis

Collecting terms of order ε^2 in Eq. (11) we find

$$D_0^2 P_2 + 2D_0 D_1 P_1 - \bar{k}\frac{\partial^2 P_2}{\partial x^2} - \bar{\alpha}_1 P_2 + 3\bar{\alpha}_2(P_0 P_1^2 + P_0^2 P_2) = 0. \tag{17}$$

A solution for P_2 is obtained by taking $\frac{\partial A(t_1)}{\partial t_1} = 0$ in Eq. (13) and P_2 of the form

$$\begin{aligned}P_2 = B_0(t_1) + C_0(t_1)\cos\left(\frac{2n\pi x}{N}\right) \\ + \left[B_{2\omega}(t_1) + C_{2\omega}(t_1)\cos\left(\frac{2n\pi x}{N}\right)\right]e^{i2\omega t_0} \\ + \left[B_{2\omega}^*(t_1) + C_{2\omega}^*(t_1)\cos\left(\frac{2n\pi x}{N}\right)\right]e^{-i2\omega t_0},\end{aligned} \tag{18}$$

where the linear frequency $\omega = \sqrt{2\bar{\alpha}_1 + \bar{k}(\frac{n\pi}{N})^2}$. The P_2 correction then only involves zero-frequency and 2ω-frequency terms. Substituting P_i for $i = 0, 1, 2$ into Eq. (17) and collecting terms of the same frequency, we find

$$B_0 = -\frac{3}{2}\sqrt{\frac{\bar{\alpha}_2}{\bar{\alpha}_1}}|A|^2, \tag{19a}$$

$$C_0 = \frac{3\sqrt{\bar{\alpha}_1\bar{\alpha}_2}|A|^2}{\left(\frac{2n\pi}{N}\right)^2\bar{k} + 2\bar{\alpha}_1}, \tag{19b}$$

$$B_{2\omega} = \frac{3}{2}\frac{\sqrt{\bar{\alpha}_1\bar{\alpha}_2}A^2}{4\omega^2 - 2\bar{\alpha}_1}, \tag{19c}$$

$$C_{2\omega} = \frac{3}{2}\frac{\sqrt{\bar{\alpha}_1\bar{\alpha}_2}A^2}{-4\omega^2 + \left(\frac{2n\pi}{N}\right)^2\bar{k} + 2\bar{\alpha}_1}, \tag{19d}$$

where $A=A(t_2,t_3,\ldots)$ so that B_0, C_0, $B_{2\omega}$, and $C_{2\omega}$ are independent of t_1.

Collecting terms of order ε^3 in Eq. (11) gives

$$D_0^3P_3 - \bar{k}\frac{\partial^2 P_3}{\partial x^2} - \bar{\alpha}_1P_3 + 3\bar{\alpha}_2P_0^2P_3 = -2D_0D_2P_1 - \hat{\gamma}D_0P_1 - \bar{\alpha}_2[P_1^3 + 6P_0P_1P_2] + [\hat{E}_0 + \hat{E}_1\sin(\pi x)]\cos(\Omega t_0), \tag{20}$$

where use is made of the fact that $D_1P_2=D_1^2P_1=0$. Substituting $P_0=\sqrt{\frac{\bar{\alpha}_1}{\bar{\alpha}_2}}$ and P_1 and P_2 from Eqs. (13) and (18) into Eq. (20), multiplying by $X_1(x)e^{-i\omega t_0}$, and integrating over $t_0\in[-\infty,\infty]$ and $x\in[0,N]$ gives

$$i\omega\left(\frac{A'}{A}+\frac{\hat{\gamma}}{2}\right) = 3\bar{\alpha}_2|A|^2\left\{1+\frac{6\bar{\alpha}_1^2}{\left[\bar{k}\left(\frac{2n\pi}{N}\right)^2+2\bar{\alpha}_1\right]\left[\bar{k}\left(\frac{2n\pi}{N}\right)^2+6\bar{\alpha}_1\right]}\right\} + \frac{1}{2}\left\{\frac{\hat{E}_0}{n\pi}[1-(-1)^n]+\frac{\hat{E}_1}{2}\delta_{n,N}\right\}\frac{A^*}{|A|^2}e^{i\Omega_0t_2}, \tag{21}$$

where $A'=\frac{\partial A(t_2)}{\partial t_2}$. Equation (21) is the condition needed to remove contributions on the left-hand side of Eq. (20) which would give rise to singularities in the solution of Eq. (20).

Writing $A(t_2)$ in the form

$$A(t_2) = \frac{1}{2}\sigma(t_2)e^{i\theta(t_2)} \tag{22}$$

for real σ and θ and substituting in Eq. (21), we find from the real part of Eq. (21)

$$-\omega\theta' = \frac{3\bar{\alpha}_2\sigma^2}{4}\left\{1+\frac{6\bar{\alpha}_1^2}{\left[\bar{k}\left(\frac{2n\pi}{N}\right)^2+2\bar{\alpha}_1\right]\left[\bar{k}\left(\frac{2n\pi}{N}\right)^2+6\bar{\alpha}_1\right]}\right\} + \frac{1}{2}\left\{\frac{\hat{E}_0}{n\pi}[1-(-1)^n]+\frac{\hat{E}_1}{2}\delta_{n,N}\right\}\frac{\cos(\theta-\Omega_0t_2)}{\sigma} \tag{23}$$

and from the imaginary part of Eq. (21)

$$\sigma' = -\frac{\hat{\gamma}}{2}\sigma - \frac{1}{2}\left\{\frac{\hat{E}_0}{n\pi}[1-(-1)^n]+\frac{\hat{E}_1}{2}\delta_{n,N}\right\}\frac{\sin(\theta-\Omega_0t_2)}{\omega}, \tag{24}$$

where $\theta'=\frac{\partial\theta}{\partial t_2}$ and $\sigma'=\frac{\partial\sigma}{\partial t_2}$. We now discuss the solutions of Eqs. (23) and (24) for a number of cases of interest.

Case I. $\hat{E}_0=\hat{E}_1=\hat{\gamma}=0$

In the case that $\hat{E}_0=\hat{E}_1=\hat{\gamma}=0$, σ is a constant and

$$\theta = -\varepsilon^2\frac{3\bar{\alpha}_2\sigma^2}{4\omega}\left\{1+\frac{6\bar{\alpha}_1^2}{\left[\bar{k}\left(\frac{2n\pi}{N}\right)^2+2\bar{\alpha}_1\right]\left[\bar{k}\left(\frac{2n\pi}{N}\right)^2+6\bar{\alpha}_1\right]}\right\}t. \tag{25}$$

Consequently, the nonlinear frequency, ω_{NL}, arising from the linear frequency $\omega=\sqrt{2\bar{\alpha}_1+(\frac{n\pi}{N})^2\bar{k}}$ is given by

$$\omega_{NL} = \omega - \varepsilon^2\frac{3\bar{\alpha}_2\sigma^2}{4\omega}\left\{1+\frac{6\bar{\alpha}_1^2}{\left[\left(\frac{2n\pi}{N}\right)^2\bar{k}+2\bar{\alpha}_1\right]\left[\left(\frac{2n\pi}{N}\right)^2\bar{k}+6\bar{\alpha}_1\right]}\right\}. \tag{26}$$

Case II. $\hat{E}_0=\hat{E}_1=0$ and $\bar{\gamma}\neq 0$

In this case, the solution of Eq. (24) gives

$$\sigma = \sigma_0e^{-\hat{\gamma}\varepsilon^2t/2} = \sigma_0e^{-\bar{\gamma}t/2} \tag{27}$$

so that from Eqs. (22), (23), and (25) we find for small $\bar{\gamma}=\hat{\gamma}\varepsilon^2$ that

$$A = \frac{1}{2}\sigma_0e^{i[\omega_{NL}+i\hat{\gamma}\varepsilon^2/2]t}. \tag{28}$$

The resulting nonlinear frequency of the plane-wavelike modes is complex, given by

$$\omega_{NL}(\hat{\gamma}\neq 0) = \omega_{NL}(\hat{\gamma}=0)|_{\sigma=\sigma_0} + i\frac{\bar{\gamma}}{2}, \tag{29}$$

where $\omega_{NL}(\hat{\gamma}=0)$ is from Eq. (26).

Case III. $\hat{E}_0$, $\hat{E}_1\neq 0$, and $\bar{\gamma}=0$

For this case it is useful to define $\varphi=\theta-\Omega_0t_2$ so that Eqs. (23) and (24) become

$$\varphi' = -\Omega_0 - Q\sigma^2 - R\cos\varphi/\sigma \tag{30}$$

and

$$\sigma' = -R\sin\varphi, \tag{31}$$

where

$$Q = \frac{3}{4}\frac{\bar{\alpha}_2}{\omega}\left\{1+\frac{6\bar{\alpha}_1^2}{\left[\bar{k}\left(\frac{2n\pi}{N}\right)^2+2\bar{\alpha}_1\right]\left[\bar{k}\left(\frac{2n\pi}{N}\right)^2+6\bar{\alpha}_1\right]}\right\} \tag{32}$$

and

$$R = \frac{1}{2\omega}\left\{\frac{\hat{E}_0}{n\pi}[1-(-1)^n]+\frac{\hat{E}_1}{2}\delta_{n,N}\right\}. \tag{33}$$

In the limit that $\Omega_0 \gg |Q\sigma^2+R\cos\varphi/\sigma|$ the solution of Eqs. (30) and (31) gives $\theta=\theta_0$ and $\sigma=\sigma_0-\frac{R}{\Omega_0}\cos(\theta_0-\Omega_0t_2)$, where σ_0 and θ_0 are constants. The time dependence of the fields is just impressed on the amplitude of A.

Another interesting limit is given by the fixed points of the system in Eqs. (30) and (31). For $\varphi'=\sigma'=0$ we find the fixed points at $\varphi=\theta-\Omega_0t_2=m\pi$ for $m\in I$ and σ given by the solutions of the cubic equation, $Q\sigma^3+\Omega_0\sigma+(-1)^mR=0$. For

these fixed point solutions the angular variable in A is $\theta = m\pi + \Omega_0 t_2$ and σ are from the real solutions of the cubic equation. Some important simple cases are: (a) in the limit that $|\sigma| \ll |\frac{R}{Q}|^{1/3}$, $\sigma = (-1)^{m+1} R/\Omega_0$ and (b) in the limit that $\Omega_0 \ll |QR^2|^{1/3}$, $\sigma = (-1)^{m+1} \frac{R}{Q} |\frac{Q}{R}|^{2/3}$. These give fixed points for high-frequency and low-frequency driving fields, respectively. The stability of these fixed points is easily determined by linearizing about them in Eqs. (30) and (31). At the fixed point (σ_0, φ_0), we find linearized solutions of the form $\varphi - \varphi_0 = \delta\varphi_0 \exp(\pm\sqrt{BC}t)$ and $\sigma - \sigma_0 = \pm \frac{\sqrt{BC}}{B} \delta\varphi_0 \exp(\pm\sqrt{BC}t)$, where $B = [-2\sigma_0^3 Q + (-1)^m R]/\sigma_0^2$, $C = (-1)^{m+1} R$, and $\delta\varphi_0$ sets the amplitude of the displacement from the fix point at $t=0$.

D. ILM

In this section we consider the discrete form of the equations from Eq. (2) describing the array of domains.[16,17] These equations are important in the limit that the space wave functions of the excitations in the system change rapidly over length scales comparable to the domain widths. This is expected to be the case for ILM that are highly localized pulses. The pulse intensity of ILM solutions uses the nonlinearity of the media to create a self-consistent change in the environment which in turn supports the localized pulse intensity.

In the notation of Eq. (4), the equations of motion, from Eq. (2), for the discrete domains in the absence of external fields becomes

$$\ddot{P}_n - \bar{\alpha}_1 P_n + \bar{\alpha}_2 P_n^3 - \bar{k}(P_{n+1} - 2P_n + P_{n-1}) = 0. \quad (34)$$

Discrete, intrinsic localized mode solutions are obtained from Eq. (34) by writing $P_n = \sqrt{\frac{\bar{\alpha}_1}{\bar{\alpha}_2}} + S_n$, where at equilibrium $P_n = \sqrt{\frac{\bar{\alpha}_1}{\bar{\alpha}_2}}$ and $S_n = S_{0,n} e^{-i\omega t} + \text{c.c.}$ is the deviation from equilibrium that arises from the presence of an intrinsic localized mode of frequency ω. Following Sievers and Page[17] we look for an intrinsic localized mode solution of the form

$$S_{0,0} = \alpha, \quad (35)$$

$$S_{0,n} = \alpha(-1)^n A e^{-(|n|-1)q}, \quad \text{for } |n| \geq 1. \quad (36)$$

This form supposes a highly localized pulse in the system with parameters fixed by the difference equations of Eq. (34). Substituting Eqs. (35) and (36) into Eq. (34) for $n=0$, 1, and $n \to \infty$, gives three nonlinear equations[17] for A, e^{-q}, and ω. These equations are

$$\cosh q - A = \frac{3\bar{\alpha}_2}{2\bar{k}} \alpha^2, \quad (37a)$$

$$\bar{k}[Ae^q - 1] = 3\bar{\alpha}_2 \alpha^2 A^3, \quad (37b)$$

and

$$\omega^2 = 2\bar{\alpha}_1 + 2\bar{k}[1 + \cosh q]. \quad (37c)$$

Equations (37) are solved for the envelope parameters of the wave function and the mode frequencies, ω, as functions of α, $\bar{\alpha}_1$, and $\bar{k}$.

IV. RESULTS AND DISCUSSION

In this section the formulas obtained in Sec. III are evaluated for lithium niobate and its various impurity structures studied in Refs. 4, 11, and 12. Considerations are given to both the MTSA for wavelike modes and the ILM solutions. A focus is on the effects of impurities in inhomogeneous ferroelectrics as these are of great current interest for possible device applications. Systems both in the absence and in the presence of an external driving term of the form $E = E_0 \cos \omega t$ are treated for temperatures well below the Curie point, e.g., at room temperature. In this limit thermal fluctuations are minimized.

First results in the linear limit of the system are considered. This is followed by a treatment of the MTSA of the fully nonlinear system and finally by ILM results.

A. Linear regime

In the linear regime the modal dispersion is given by $\omega_L^2 = 2\bar{\alpha}_1 + \bar{k}(\frac{n^2\pi^2}{N^2})$, where $n = 1, 2, \ldots, N$ and N is the number of domains in the array. An idea of the value of $\bar{\alpha}_1$ is obtained using the parameters in Ref. 7 for lithium niobate with an impurity concentration of 0.133 mol. %.[11,12] We find $\alpha_1 = 1.8849 \times 10^9$ V mC^{-1}, $E_c = 40$ kV/cm, and $P_s = 0.75$ C/m^2 giving a value for the dimensionless parameter $\bar{\alpha}_1 = 353.42$. Values of $\bar{k}$ are more difficult to estimate, but it is found that the results for the system are not overly sensitive to $\bar{k}$ over a significant range. (This point will be addressed again in Sec. IV B.) In addition, we shall assume that the dependence of $\bar{k}$ on impurity concentration is the same as that for the switching field, E_c. This is not unreasonable as both of these parameters measure similar responses of the array of domains to changes in the domain polarization. Results are presented assuming a range of $\bar{k} \approx 10$ and ≈ 100, demonstrating the lack of sensitivity in $\bar{k}$ and at the same time showing the qualitative behaviors expected in the system. In addition, lithium niobate exists in various states of intrinsic defect concentrations, displaying a concentration-dependent E_c. This is the origin of a concentration dependence in $\bar{\alpha}_1$. We shall take into account the concentration dependence of $\bar{\alpha}_1$ through E_c which has recently been measured by Yan, *et al.*[12] These authors found a large set of experimental data points for E_c fit by the general form

$$E_c = 114.(x - 0.06)^{1/3}. \quad (38)$$

Here E_c is in kilovolt per centimeter and $0.0 \leq x \leq 1.0$ is the molar % concentration of $\text{Nb}_{\text{Li}}^{4+}$ defects. Both Eq. (38) and the experimental data points for E_c given by Yan *et al.*[12] are used in our later discussions. The values of α_1 and P_s given above will be assumed to be independent of x.

In Fig. 2 the linear frequency modes are presented versus x for a series of n/N, with results shown for a system in which $\bar{\alpha}_1 = \bar{\alpha}_2$ (see the end of Sec. II). The lines in the figure are obtained from Eq. (38) and the points are obtained using the experimental data given in Yan *et al.*[12] The data from Ref. 12 use to obtain the points in Fig. 2 and later in Fig. 3 are shown in Table I. The results in Fig. 2(a) are for $\bar{k} = 10$

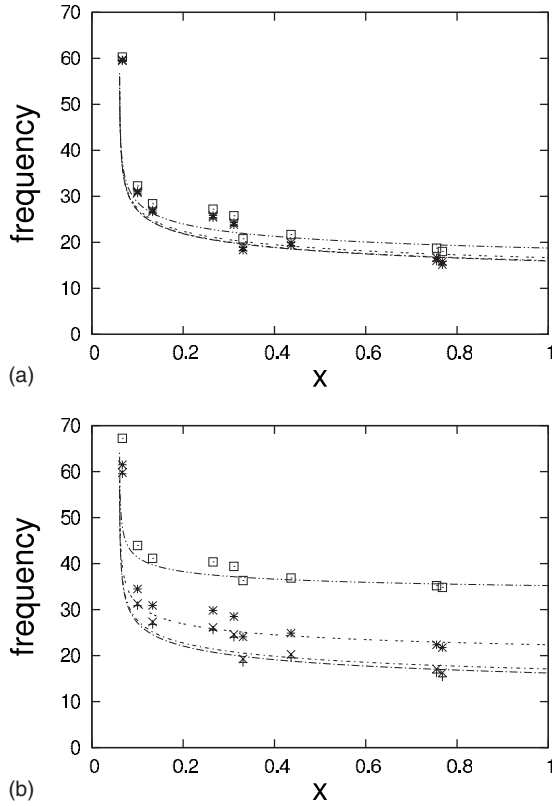

FIG. 2. The linear limit of the frequency of the normal modes of vibrations versus the impurity concentration (mole%) in lithium niobate given by x. The points are from the data points of Yan *et al.* (Ref. 12) and the lines are from Eq. (38). In (a) results are for $\bar{k}=10$ with $n/N=0.1$, 0.2, 0.5, and 1.0 from bottom to top and in (b) results are for $\bar{k}=100$ with $n/N=0.1$, 0.2, 0.5, and 1.0 from bottom to top. For a fixed x, results for the Yan, *et al.* data points (see Table I) with different point styles are for $n/N=0.1$, 0.2, 0.5, and 1.0 from bottom to top.

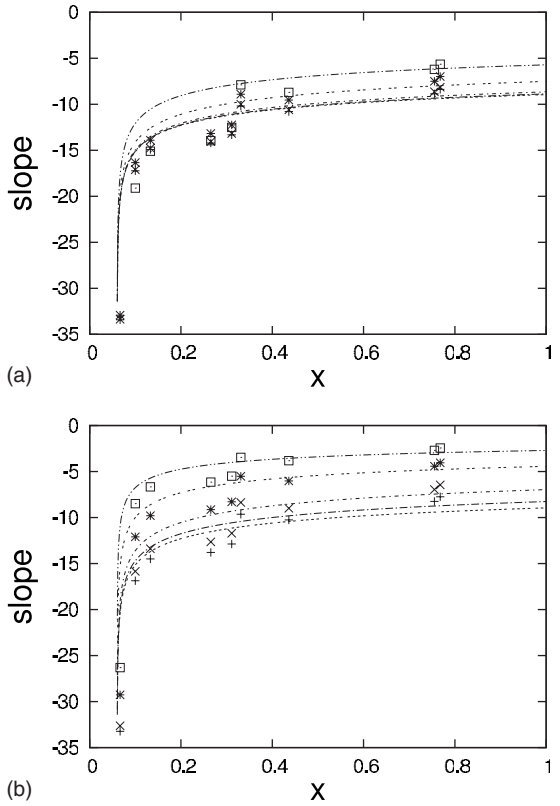

FIG. 3. Plot of the slope, $\frac{1}{\varepsilon^2}\frac{d\omega_{NL}}{d\sigma^2}$, versus the impurity concentration (mole%) in lithium niobate given by x. The points and lines are as Fig. 2. In (a) results are for $\bar{k}=10$ with $n/N=0.1$, 0.2, 0.5, and 1.0 from bottom to top and in (b) results are for $\bar{k}=100$ with $n/N=0.1$, 0.2, 0.5, and 1.0 from bottom to top. For a fixed x, results for the Yan *et al.* data points (see Table I) with different point styles are for $n/N=0.1$, 0.2, 0.5, and 1.0 from bottom to top. In both plots the lower limiting curve of $\frac{1}{\varepsilon^2}\frac{d\omega_{NL}}{d\sigma_2}$ for $\bar{k}=0$ are presented. For the scale of the plot in Fig. 3(a), the $n/N=0.1$ and $\bar{k}=0$ curves cannot be distinguished.

and those in Fig. 2(b) are for $\bar{k}=100$. In Fig. 2(a) modes are presented for $n/N=0.1$, 0.2, 0.5, and 1.0. At fixed concentration the frequency is seen to increase with increasing n/N. In Fig. 2(b) modes are presented for $n/N=0.1$, 0.2, 0.5, 1.0, and again at a fixed concentration the frequency increases with increasing n/N. In both cases the linear frequency modes are insensitive to x until the immediate neighborhood of $x \approx 0.06$ is approached. From Eq. (38) it is seen that $E_c \to 0$ in this limit. In both figures, for finite N, the frequency spectrum at fixed x is a discrete set of N different frequencies within the range $\sqrt{2\bar{\alpha}_1} < \omega_L \leq \sqrt{2\bar{\alpha}_1 + \bar{k}\pi^2}$.

In Fig. 2 for $x \leq 0.1$, the frequency of the modes sharply decrease with increasing impurity content. This region corresponds to values of $E_c \leq 40$ kV/cm which are values that Gopalan and co-workers[4] found easiest to work with in their studies of the hysteresis of samples of the appropriate thicknesses. Outside this region, at larger impurity concentrations, the curves slowly decrease in frequency with increasing concentration. The sharp fall of mode frequency in the region of low impurity concentration correlates with the onset of domain pinning. This correlation follows from the parameter $\bar{\alpha}_1 = \alpha_1 P_s / E_c$ where the x dependence of the frequency enters through the functional dependence of E_c. As the rotation of the domains becomes difficult, the coercive field E_c increases, and (as we see) the mode frequencies soften. Consequently, an analysis of the linear modes of vibrations might act as a confirmation of stiffening of domain rotation.

TABLE I. Data for Ref. 12 used to generate points shown in Figs. 2 and 3. E_c is in kilovolt per centimeter.

x_1	E_c	$\bar{\alpha}_1$
0.06658	8.0	1767.09
0.09998	30.0	471.23
0.13298	40.0	353.42
0.26525	44.0	321.29
0.31114	50.0	282.74
0.33113	85.0	166.31
0.43616	76.0	186.01
0.75509	112.0	126.22
0.76802	125.0	113.09

B. Nonlinear plane-wavelike modes

In this section results are presented for the nonlinear cases I, II, and III of plane-wavelike modes in the lithium niobate system. These modes evolve from the linear limit of the system and are renormalized by the nonlinearity. Due to the nonlinear terms in the Hamiltonian, the frequencies of the plane-wavelike modes depend on their mode amplitudes. This behavior is illustrated in the plots given in Fig. 3 for the corrections to the linear frequencies arising from the nonlinearity of representative plane-wavelike modes.

In Fig. 3 results from Eq. (26) for the slope, $\frac{1}{\varepsilon^2}\frac{d\omega_{NL}}{d\sigma^2}$, of the nonlinear frequency with respect to the squared modulus of the wave amplitude are plotted against the impurity concentration for a system with $\bar{\alpha}_1=\bar{\alpha}_2$. The plots are made of curves labeled by n/N using the same parameters as in Fig. 2, and the results in Figs. 3(a) and 3(b) are for $\bar{k}=10$ and 100, respectively. [Note: for our later discussions, the lower limiting curve for $\bar{k}=0$ is also presented in Figs. 3(a) and 3(b).] For both $\bar{k}=10$ and 100 it is seen that, at a fixed concentration, the absolute value of the slope of the nonlinear frequency decreases with increasing mode index so that the effects of the nonlinearity decreases with an increase in n/N. This is understood physically as follows. The space dependence of the nth mode is given by $\sin(\frac{n\pi x}{N})$ over $x\in[0,N]$ so that $P\propto\sin(\frac{n\pi x}{N})$ in Eq. (4). The nonlinear source term in Eq. (4) is then proportional to $P^3\propto\sin^3(\frac{n\pi x}{N})$ so that as n/N increases, the oscillations of P^3 over a fixed interval of $x\in[0,N]$ tend to average to a net zero effect. This decreases the effects of the P^3 term on the system properties for increasing n.

The absolute values of the slopes are also found to increase rapidly as E_c approaches zero for percentage impurity concentrations less than $x=0.1$. Above these concentrations (i.e., for $x>0.1$) the slope shows a mild concentration dependence. Again, as with the linear frequency modes, the behavior of the slope corrections for the nonlinearity correlate with E_c and the concentration dependence of the slope arises solely from the concentration dependence of E_c. The absolute value of the slope, for a fixed concentration, exhibits a mild decrease with increasing $\bar{k}$ so that as the coupling between the domains is increased the effects of the nonlinearity on the dispersion relation are decreased. As discussed in Sec. III, the effects of dissipation (entering through $\hat{\gamma}$) can be easily accounted for by adding a complex term.

As an indication of the moderate influence of the value of $\bar{k}$ on our perturbation results, consider the $\bar{k}=0$ and $\bar{k}\to\infty$ limits of Eq. (26). With $\bar{k}=0$ we find that the slope $\frac{1}{\varepsilon^2}\frac{d\omega_{NL}}{d\sigma^2}=-\frac{9}{8}\sqrt{\frac{\bar{\alpha}_1}{2}}$, and when $\bar{k}\to\infty$ the slope $\frac{1}{\varepsilon^2}\frac{d\omega_{NL}}{d\sigma^2}\to 0$. In both Figs. 3(a) and 3(b) we have plotted as a function of x the $\bar{k}=0$ curve of $\frac{1}{\varepsilon^2}\frac{d\omega_{NL}}{d\sigma^2}$. This curve gives the lower bound of the slope as functions of $\bar{k}$. The upper bound of the slope as functions of $\bar{k}$ is then given by the $\frac{1}{\varepsilon^2}\frac{d\omega_{NL}}{d\sigma^2}=0$ axis. For each value of x, $\frac{1}{\varepsilon^2}\frac{d\omega_{NL}}{d\sigma^2}$ as a function of $0\le\bar{k}<\infty$ lies within the region between these two curves. Our theory then provides for limits on the rate of change in the nonlinear frequency with changes in the amplitude treated as a function of $\bar{k}$. Another set of useful relationships is obtained by looking at these two limiting behaviors for the form given by $\frac{\omega}{\varepsilon^2}\frac{d\omega_{NL}}{d\sigma^2}$. For this form, the $\bar{k}=0$ limit gives $\frac{\omega}{\varepsilon^2}\frac{d\omega_{NL}}{d\sigma^2}=-\frac{9}{8}\bar{\alpha}_1$ and the $\bar{k}\to\infty$ limit gives $\frac{\omega}{\varepsilon^2}\frac{d\omega_{NL}}{d\sigma^2}=-\frac{3}{4}\bar{\alpha}_1$. These relationships offer a much more restrictive set of conditions on the dependence of the change in frequency with amplitude in our system. This is good as $\bar{k}$ is a phenomenological constant that depends on many of the complex features of domain-wall formation and motions which are currently a topic of much research interest for their understanding in terms of microscopic mechanisms, i.e., see Refs. 4, 5, and 12. It is hoped that our phenomenological treatment will provide, for general values of $\bar{k}$, some understanding of the limitations on the amplitude dependence of the frequency arising from these interaction.

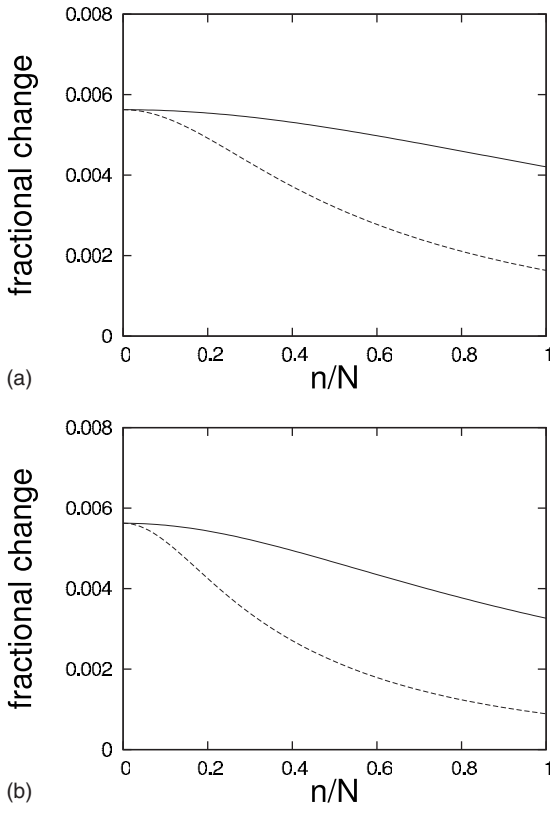

FIG. 4. Results for $(\omega_L-\omega_{NL})/\omega_L$ versus n/N for $\bar{k}=10$ (upper) and $\bar{k}=100$ (lower) for: (a) $x=0.1$ and (b) $x=0.6$.

In Fig. 4 results are presented which indicate the relative importance of the nonlinear correction term as a function of concentration. The relative change given by $(\omega_L-\omega_{NL})/\omega_L$ between the linear (denoted L) and nonlinear (denoted NL) frequencies is plotted for $\varepsilon\sigma=0.1$ as a function of n/N using Eq. (38). To make a comparison, curves are shown for $\bar{k}=10$ (upper curve) and $\bar{k}=100$ (lower curve) in Fig. 4(a) for $x=0.1$ and Fig. 4(b) for $x=0.6$. The relative corrections are found to decrease with increasing n/N, and the decrease is more pronounced with increasing $\bar{k}$.

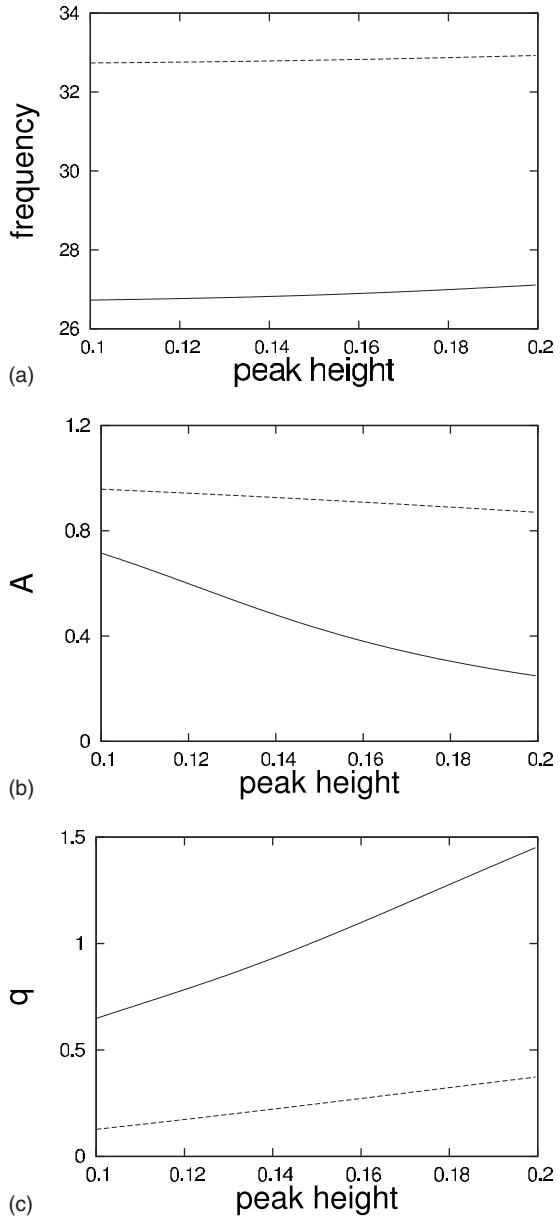

FIG. 5. Results for the intrinsic localized modes plotted as a function of the peak height, α. Plots are for: (a) the mode frequency, ω (lower line for $\bar{k}=10$ and upper line for $\bar{k}=100$), (b) the wave-function parameter, A (lower line for $\bar{k}=10$ and upper line for $\bar{k}=100$), and (c) the wave-function parameter, q(upper line for $\bar{k}=10$ and lower line for $\bar{k}=100$).

C. Nonlinear intrinsic localized modes

In Fig. 5 results are presented for the intrinsic localized modes from the solutions of Eq. (37). The solutions for the ILM mode frequency ω and the wave-function parameters A and q are given at $\bar{\alpha}_1=335$ for $\bar{k}=10$ and 100 and are plotted as functions of the mode peak height α. The total staggered polarization is given from Sec. III D by $P_n=\sqrt{\frac{\bar{\alpha}_1}{\bar{\alpha}_2}}+S_n$ so that the ILM rides on a background of uniform staggered polarization.

In Fig. 5(a) the frequency of the ILM is given as a function of ILM peak height, α, in the region $0.1\leq\alpha\leq0.2$ for both $\bar{k}=10$ (lower solid line) and $\bar{k}=100$ (upper dashed line). As a comparison, the band limits of the linear frequency modes are at the lower limit $\sqrt{2\bar{\alpha}_1}=25.9$ in both the continuum and discrete models and at the upper limit $\sqrt{2\bar{\alpha}_1+\bar{k}\pi^2}=27.7$ for $\bar{k}=10$ and 40.7 for $\bar{k}=100$ in the continuum model but at $\sqrt{2\bar{\alpha}_1+\bar{k}4}=26.65$ for $\bar{k}=10$ and 32.71 for $\bar{k}=100$ in the discrete model. The discrete model upper limit is more relevant for a comparison with the ILM dispersion in the following discussions as it contains the dispersion introduced by the discrete nature of the lattice which is important at the high-frequency edge of the band. It is found, for the data presented, that the frequencies of the ILM fall above the region of the band of linear modes in the discrete model. The ILM may then exist as an excitation separate from the plane-wave modes as it is outside the band of states. In both continuum and discrete models, the discrete frequencies of the plane-wave modes (given by the set of ratios n/N that are possible in the system) will be different from the frequency of the ILM and may not support a rapid decay of the ILM. For the limit of an infinite array of domains the increased number of modes may facilitate the decay of the ILM. As the coupling $\bar{k}$ between the domains is increased, it is seen in Fig. 5(a) that the frequency of the ILM and its band of linear modes increases, but the ILM remains at higher frequencies than the band of linear modes. The general features of the mode dispersion appear to be qualitatively independent of $\bar{k}$.

In general, the ILM are found to increase in frequency with increasing α, exhibiting a mild dependence on the peak height. This is different from the wavelike solutions which are found to decrease in frequency with increasing mode amplitude. In Fig. 5(b) the wave-function parameter A, which sets the field intensity at the sites adjacent to the maximum peak height, is presented as a function of α. The curves are for $\bar{k}=10$ (lower solid) and 100 (upper dashed). It is seen to decrease mildly with an increasing peak height of the ILM. In Fig. 5(c) the decay parameter of the wave function, q, is plotted versus α. The curves are for $\bar{k}=10$ (upper solid) and $\bar{k}=100$ (lower dashed). It is observed to increase with increasing peak height. The wave function of the intrinsic localized mode is then consistent with a highly "localized pulse excitation" with a frequency above the band of linear plane-wave excitations in the domain array. As α increases the pulse of the ILM tends to become more localized. The pulse becomes more delocalized with increasing $\bar{k}$.

V. CONCLUSIONS

Two different types of excitations in arrays of ferroelectric domains have been investigated within the context of a model of a one-dimensional array of ferroelectric slabs. These include plane-wavelike modes and pulse-type intrinsic localized modes. The model gives a simple treatment of finite arrays of domains which may typically occur in ferroelectric systems, and the qualitative behaviors it displays may be expected in types of systems that have become of interest in the context of the study of nanostructures.

The multiple-time-scale analysis was shown to give a useful insight into the linear and nonlinear plane-wave modes under different conditions of external driving force and damping. The analysis is based on the continuum limit nonlinear Klein-Gordon equation. This is a natural extension of the Landau free energy and would be valid for large domain arrays and for excitations with wavelengths larger than the typical domain size. The modes in the linear regime show an important variation with the impurity content in lithium niobate, indicating the start of stiffening of the rotation of domains and domain walls at E_c values around 40 kV/cm. This correlates with our previous work on domain-wall widths.

In the nonlinear regime, without any field and without any damping, the nonlinear frequency is found for $\bar{\alpha}_1 = \bar{\alpha}_2$ to decrease with increasing wave amplitude. This behavior is consistent with results found on nonlinear oscillators with both quadratic and cubic nonlinearities. In our model, damping enters as a simple imaginary contribution to the complex frequency and driving fields exhibit fixed point behaviors. ILM are found as localized pulses, occurring above the band limits of the finite number of plane-wavelike modes.

The present paper represents an extension of work in Refs. 5, 7, and 10 on a dynamical model for ferroelectric domains which is based on the Ginzberg-Landau free-energy form. The Ginzberg-Landau form used was taken to be appropriate to systems with second-order phase transitions, and this is why we have focused on lithium niobate systems. In addition to having a recent importance for technological applications, lithium niobate also has a set of very nice data[11,12] which facilitates the discussions of our theory. In Refs. 5 and 10 a treatment of the complex nonlinear motion of single domains, the values of E_c, and the domain-wall energies and widths between two neighboring domains in lithium niobate were given in terms a form of the Ginzberg-Landau-based theory which did not directly take into account the interactions between the separate domains. In Ref. 7 the model was generalized to include phenomenological terms for the interaction between separate ferroelectric domains and was then used in a discussion of the continuum limit of domain-wall solitons.

The present work applies the model from Ref. 7, for interactions between domains, to a system of multiple interacting ferroelectric domains and determines the nonlinear dynamics of extended wavelike modes and discrete intrinsic localized modes that exist as excitations of the array of domains. The extension in this work is then to go from a system of a single domain or a set of two domains with a focus on the interdomain wall to treat a full array of N interacting domains. The motion of the array of N ferroelectric domains discussed in this paper should be of importance to recent interests in nanoscience. Here the effects of the individual motions of the domains become visible as systems with design features that are made on increasingly smaller length scales are formulated. On such scales the modal behaviors of the domains of the system are no longer an academic concern but may be of technological importance, and our work here suggests that the nonlinearity found in the array dynamics is composed of a number of different types of excitations which can factor into such considerations. The extended waves and intrinsic localized modes have similar excitations frequencies so that both are expected to be dynamical factors of equal importance. The two types of excitations are further seen to be distinguished from one another as their frequencies renormalize in opposite ways under increasing excitation amplitude. Experimentally speaking, this should be valuable in distinguishing between these two types of excitations in the system. Since our model is only restricted in its considerations to systems based on the Ginzberg-Landau form for second-order phase transitions, we expect that the qualitative nature of the solutions presented here for lithium niobate carry over to other systems that have second-order phase transitions. Our results should be qualitatively found in all such systems.

ACKNOWLEDGMENT

The authors (A.K.B. and P.C.R.) would like to thank V. Gopalan of Dept. of Materials Science and Engineering at Penn State University (USA) for providing some experimental data and useful discussion.

*asisbanerjee1000@yahoo.co.in
†raypratap1@yahoo.co.in
‡vu-quoc@ufl.edu
§Corresponding author; arthur.mcgurn@wmich.edu

[1] *Principle and Application of Ferroelectric and Related Materials*, edited by M. E. Lines and A. M. Glass (Clarendon, Oxford, 1977).
[2] F. Jona and G. Shirane, *Ferroelectric Crystals* (Pergamon, Oxford, London, 1962).
[3] H. Fu and R. E. Cohen, Nature (London) **403**, 281 (2000).
[4] S. Kim, V. Gopalan, and A. Gruverman, Appl. Phys. Lett. **80**, 2740 (2002).
[5] A. K. Bandyopadhyay and P. C. Ray, J. Appl. Phys. **95**, 226 (2004).
[6] V. Srinivas and L. Vu-Quoc, Ferroelectrics **163**, 29 (1995).
[7] A. K. Bandyopadhyay, P. C. Ray, and V. Gopalan, J. Phys.: Condens. Matter **18**, 4093 (2006).
[8] A. K. Bandyopadhyay, P. C. Ray, and V. Gopalan, Eur. Phys. J. B **65**, 525 (2008).
[9] *Nanoelectronics and Information Technology*, edited by Rainer Waser (Wiley, Weinhiem, 2005).
[10] A. K. Bandyopadhyay, P. C. Ray, and V. Gopalan, J. Appl. Phys. **100**, 114106 (2006).
[11] L. Tian, V. Gopalan, and L. Galambos, Appl. Phys. Lett. **85**, 4445 (2004).
[12] W. Yan, Yongfa Kong, Lihong Shi, Lei Sun, Hongde Liu, Xiaochun Li, Di Zhao, Jingjun Xu, Shaolin Chen, Ling Zhang, Ziheng Huang, Shiguo Liu, and Guangyin Zhang, J. Phys. D **39**, 21 (2006).
[13] A. H. Nayfeh, *Introduction to Perturbation Technique* (Wiley,

New York, 1981).
[14] S. K. Das, P. C. Ray, and G. Pohit, J. Vib. Control **11**, 1511 (2005).
[15] J. W. Fleischer, M. Segev, N. K. Elfremidis, and D. N. Christodoulides, Nature (London) **422**, 147 (2003).
[16] M. Sato, B. E. Hubbard, and A. J. Sievers, Rev. Mod. Phys. **78**, 137 (2006).
[17] A. J. Sievers and J. B. Page, in *Dynamical Properties of Solids*, edited by G. K. Horton and A. A. Maradudin (North-Holland, Amsterdam, 1995), Vol. 7.
[18] S. Baroni, S. D. Gironcoli, and A. D. Corso, Rev. Mod. Phys. **73**, 515 (2001).
[19] M. Lazzeri and S. de Gironcoli, Phys. Rev. Lett. **81**, 2096 (1998).
[20] Ph. Ghosez, X. Gonze, and J. P. Michenaud, Ferroelectrics **206**, 205 (1998).
[21] Ph. Ghosez, J. P. Michenaud, and X. Gonze, Phys. Rev. B **58**, 6224 (1998).
[22] Yu. S. Kivshar and M. Peyrard, Phys. Rev. A **46**, 3198 (1992).
[23] Y. S. Kivshar, A. R. Champneys, D. Cai, and A. R. Bishop, Phys. Rev. B **58**, 5423 (1998).
[24] K. Forinash and C. R. Willis, Physica D **2598**, 1 (2000).
[25] C. J. Brennan and K. A. Nelson, J. Chem. Phys. **107**, 9691 (1997).
[26] S. Flach and A. V. Gorbach, Phys. Rep. **467**, 1 (2008).